

RSC Advances



This is an *Accepted Manuscript*, which has been through the Royal Society of Chemistry peer review process and has been accepted for publication.

Accepted Manuscripts are published online shortly after acceptance, before technical editing, formatting and proof reading. Using this free service, authors can make their results available to the community, in citable form, before we publish the edited article. This *Accepted Manuscript* will be replaced by the edited, formatted and paginated article as soon as this is available.

You can find more information about *Accepted Manuscripts* in the [Information for Authors](#).

Please note that technical editing may introduce minor changes to the text and/or graphics, which may alter content. The journal's standard [Terms & Conditions](#) and the [Ethical guidelines](#) still apply. In no event shall the Royal Society of Chemistry be held responsible for any errors or omissions in this *Accepted Manuscript* or any consequences arising from the use of any information it contains.

Covalent Synthesis of Perylenediimide-Bridged Silsesquioxane Nanoribbons and Their Electronic Properties

Lan Xu^a, Venkata Ramana Manda^a, Louis E. McNamara^b, Muhammad P. Jahan^c, Hemali Rathnayake^{a}, Nathan I Hammer^{b*}*

Abstract. Perylenediimide-functionalized silsesquioxane nanostructures were prepared from base-catalyzed polymerization of their respective monoalkoxysilane precursor. The shapes of nanostructures varied from nanoribbons to nanochains to nanorods upon changing the base concentration. Transmission electron microscopy confirms the twisted nature of nanoribbons with lengths up to 15 μm , whereas the dimensions of nanorods were in the range of 9 μm in length and 200 nm in width. The photovoltaic performance of the nanoribbons and nanorods were evaluated and compared for bulk heterojunction solar cells and it was discovered that morphology plays an important role in the PV performance.

Introduction

The hierarchical assembly of nanoscale building blocks with tunable dimensions and structural complexities is essential for controlling the distinctive geometry of 1D-structures. Such nanomaterials are utilized for a variety of nanostructure applications, including high-strength nanocomposites, field-emitting surfaces, sensors, nanotransistors, biomaterial delivery tools,

optical devices, electrode materials, energy storage devices, and catalysts.¹⁻⁹ Great efforts have been made to develop techniques to produce unique 1D-structures, such as laser-assisted catalytic growth,¹⁰ solution–liquid–solution techniques,¹¹ template directed synthesis,¹² and self-assembly processes from noncovalent interactions.^{13,14}

Among different types of 1D-nanomaterials, organic nanostructures have gained interest due to their distinct optical, electrical, and mechanical properties.^{8-9,15} The general method of preparing organic nanomaterials is through noncovalent interactions such as hydrogen bonding, π - π stacking, and solvophobic and surface effects.¹⁶⁻²¹ To date, a variety of supramolecular architectures has been fabricated by molecular self-assembly of tailored, supramolecular building blocks.²²⁻²⁸

Significant research efforts have been reported for the self-organization of perylenediimides (PDIs) into 1D-structures such as nanofibers, nanowires, and nanoribbons.^{14,29-33} The planar π -conjugated aromatic framework of PDIs make them ideal moieties for supramolecular self-assembly into discrete nanomaterials through strong π - π interactions. To fabricate PDIs into 1D nanostructures through self-assembly, cofacial π - π stacking is beneficial. Zhang and co-workers have demonstrated that cofacial π - π stacking between molecular skeletons requires the assembly of PDI into 1D structures.³⁴ A variety of techniques such as phase transfer, solvent annealing, vapor diffusion, and seeded growth were introduced to generate nanobelt, nanowires, and nanofibers from PDI systems that would otherwise form bulky aggregates.³³⁻³⁵

Achieving nanosized structures with distinct geometries via self-organization processes, however, is a great challenge and has limited control over the morphology of the final structure. For example, PDI-nanowires prepared using solvent aggregation show wide distribution of dimensionalities and have limited access to manipulate their chain growth.³³ Alternatively, the

covalent synthesis is an advantage over self-assembly processes for making well-defined three-dimensional nanostructures with controlled morphologies upon controlling the concentration of reactants which determine the chain lengths and geometries. Herein, we demonstrate a novel method to prepare 1D-nanostructures varied from nanoribbons to nanochains to nanorods via covalent synthesis. The work described here is a unique example for the preparation of nanostructures with controlled geometries by manipulating the base concentration during the polymerization process. As depicted in Figure 1, perylenediimide-functionalized bridged silsesquioxane nanoribbons, nanochains, and nanorods were prepared by base-catalyzed hydrolysis and condensation from their respective organomonoalkoxydisilane precursor. Upon changing the base concentration, the resulting morphology varies from nanoribbons to nanorods to nanochains. The polymerized structure of perylenediimide units interconnects one another through Si-O-Si bridging units to give PDI-bridged silsesquioxane network (PDIB-silsesquioxanes). The methods developed here build on our previously published work on preparing poly(3-hexylthiophene)- and perylenediimide- functionalized silsesquioxane nanoparticles.^{36,37}

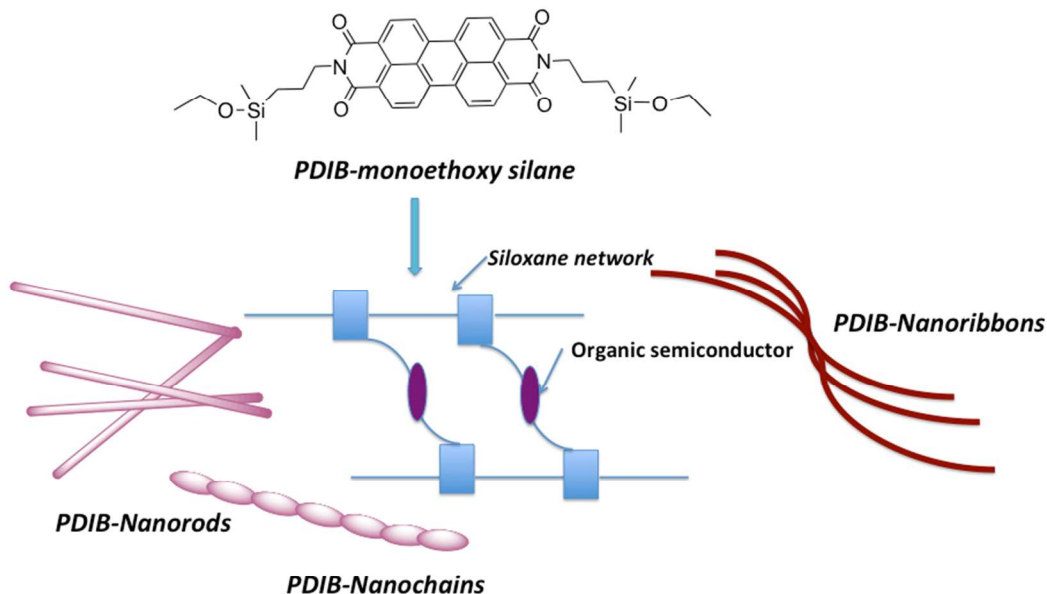


Figure 1. Schematic representation illustrating PDI-nanostructures prepared from PDI-functionalized silane precursors.

The focus of this work is to investigate how different morphologies affect the resulting optoelectronic properties of these materials, including their photovoltaic performances for bulk heterojunction solar cells. By comparing the photophysical properties of these materials in the solution phase, in thin-film morphologies, and at the single nanostructure level, the effect of architecture on the resulting properties of PDIB-nanostructures is revealed. Additionally, the photovoltaic performances of PDIB-nanoribbons and nanorods are also evaluated by blending them with a donor polymer, poly(3-hexylthiophene).

Experimental

Materials: 3,4,9,10-tetracarboxydianhydrideperylene, regioregular-poly(3-hexylthiophene) (average M_n 30,000 - 60,000 g/mol), anhydrous ethanol (200 proof), chloroform (HPLC grade), and chlorobenzene (HPLC grade) were obtained from Aldrich chemicals. Ammonium hydroxide (28%) was obtained from Fischer Scientific. 3-aminopropyldimethylethoxy silane was purchased from Gelest Inc. Unless otherwise specified, all chemicals were used as received.

Characterization: Proton NMR spectra were recorded on a 500 MHz JEOL using $CDCl_3$ as a solvent. FTIR spectra were acquired using a Perkin-Elmer Spectrum One FT-IR spectrometer equipped with a universal ATR sampling accessory. Transmission electron microscopy (TEM) observations were performed on a 100CX JEOL at 80 keV. The elemental compositions (C, H, and N) of the silane precursor were analyzed by the Micro-Elemental Analysis Lab at Advanced Materials Institute, Western Kentucky University. The photophysical properties in solution were studied using a fluorescence spectrometer (Perkin Elmer LS 55) and UV-visible spectrometer (Perkin Elmer, Lambda 35). The contact mode atomic force microscopy (AFM) topographic images were obtained using an Agilent 5500AFM using a silicon probe coated with aluminum

(contact G-10). Thin films were prepared by spin coating PDIB-nanoribbons (8 mg/mL in chlorobenzene) onto plasma cleaned glass slides ($2 \times 2 \text{ cm}^2$) to give a film thickness of $\sim 100 - 150 \text{ nm}$. The test devices for electrical conductivity measurements were prepared on pre-cleaned ITO glass by spin coating the solutions of nanoribbons (10 mg/mL in chlorobenzene) and PDI-dimethyl silane (10 mg/mL in chlorobenzene) followed by deposition of Al ($\sim 80 \text{ nm}$) as the cathode. The device area used was $2 \times 6 \text{ mm}^2$.

Thin film and single nanostructure emission spectra were acquired using a Nikon Eclipse TE2000-U inverted microscope with a 1.4 numerical aperture objective and Ar^+ laser excitation with EMCCD camera detection (Princeton Instruments ProEM 1024). Excited state lifetimes were fit using the FluoFit software package.

PDIB-dimethylethoxysilane. To a three-necked round bottom flask, 3,4,9,10-tetracarboxydianhydrideperylene (0.49 g, 1.12 mmol) and anhydrous ethanol (50.0 mL) were added and heated to reflux under argon atmosphere. Then excess 3-aminopropyldimethylethoxysilane (2.0 g, 12.4 mmol) was added and allowed to reflux for 24 hours. The resulting dark red solid was washed with hexane and ethanol to remove excess 3-aminopropyldimethylethoxysilane. The dark red solid was dissolved in chloroform ($\sim 50 \text{ mL}$) and an insoluble solid, which was later confirmed by FTIR as a mixture of 3,4,9,10-tetracarboxyanhydrideperylene and hydrolyzed perylenediimide siloxanes was removed by centrifugation and gravity filtration. The filtrate was concentrated in vacuum to yield a dark red solid (500 mg, yield = 59%). $^1\text{H-NMR}$ in CDCl_3 $\{\delta, \text{ppm}\}$: NMR, 8.49-8.47 (2H,d), 8.33-8.31 (2H, d), 4.17-4.14 (2H, t), 3.70-3.65 (2H, q), 1.82-1.76 (2H, m), 1.20-1.17 (3H, t), 0.76-0.73 (2H, t), 0.14 (16H, s); FTIR stretching (cm^{-1}): 2955-2886 (C-H stretching of alkyl chains), 1692 (diimide carbonyl stretching), 1593-1577 (aromatic C-C stretching), 1439 (N-C stretching from

perylene-diimide), 1378-1248 (Si-C stretching), 1103-1072 (Si-O-); elemental analysis (%): experimental – C 66.8, H 6.26, N 4.04; Calculated – C 67.2, H 6.2, N 4.1.

Typical procedure for the preparation of PDI-nanoribbons: To a 250 mL round bottom flask, the PDI-dimethylsilane monomer (~200 mg, 0.29 mmol) in chloroform (15 mL) was added through the micro-filter under argon atmosphere. Microfiltration was used to remove any additional impurities and insoluble solid particles. An anhydrous ethanol (150 mL) and ammonium hydroxide (14.45 M - 28% in water, 20 mL, 290 mmol) mixture was added slowly to form two layers and allowed to react for 48 hours. The nanoribbons were isolated by repeated centrifugation and repeated redispersion in ethanol. After being completely dried in stream air, the nanoribbons were collected as a red solid (Yield 56%). FTIR stretching (cm^{-1}): 2993-2885 (C-H stretching of alkyl chains), 1692 (diimide carbonyl stretching), 1593-1558 (aromatic C-C stretching), 1440 (N-C stretching from perylene-diimide), 1379-1250 (Si-C stretching), 1098-1016 (Si-O-).

Typical procedure for the preparation of PDI-nanorods:

To a 100 mL round bottom flask, anhydrous ethanol (37.5 mL) and ammonium hydroxide (14.45 M - 28% in water, 5 mL, 70 mmol) were added under argon atmosphere. The base concentration was adjusted to 1.48 mol/L by adding 2.5 mL of water. Then the PDI-dimethylsilane monomer (~50mg, 0.07mmol) in chloroform (3.75 mL) was slowly added through the micro-filter to the reaction mixture and stirred for 48 hours at room temperature. A majority of the nanorods remained in the supernatant after the very first centrifugation, which removes the unreacted fibrous material. After repeated centrifugation, the nanorods were collected as a red solid. The yield was low (~20%) since the nanorods were difficult to separate from the solution.

Device Fabrication. Model bulk heterojunction solar cell devices were prepared on glass/ITO substrates. The substrates were subsequently cleaned in 2-propanol and acetone in an ultrasonic bath for 15 minutes each and a layer of PEDOT:PSS (purchased from Aldrich) with a thickness of ~400-500 nm was spray-deposited as a hole transporting layer on top of ITO under a stream of nitrogen. The substrates were heated at 100°C in a vacuum oven for an hour. As a first step, the active layer of PDIB-nanostructures: P3HT (average $M_n = 30,000 - 60,000$ g/mol) dissolved in chlorobenzene (10 mg/mL concentration of each compound of 1:1 ratio) was spray-deposited to give a film thickness of 300-400 nm under a stream of nitrogen. The substrates were transported into vacuum evaporator and a layer of calcium (~2 nm) and aluminum (~50 nm) was thermally evaporated on top of the active layer with a coating of 2 x 6 mm through a mask. The final devices were annealed inside a glove box at 100 °C for five minutes and then transferred to a glass chamber under a stream of nitrogen gas and the chamber was sealed for device characterization. Testing of the devices was performed using a solar simulator with an emission spectrum close to AM 1.5G and intensity of 80 W/m². The IV curves of the devices were measured using a Keithley 2400 source meter. The fill factor (FF) and power conversion efficiency (PCE) were calculated manually using following the following two equations.

$$FF = \frac{J_m V_m}{J_{sc} V_{oc}} PCE = \frac{J_{sc} V_{oc} FF}{P_s}$$

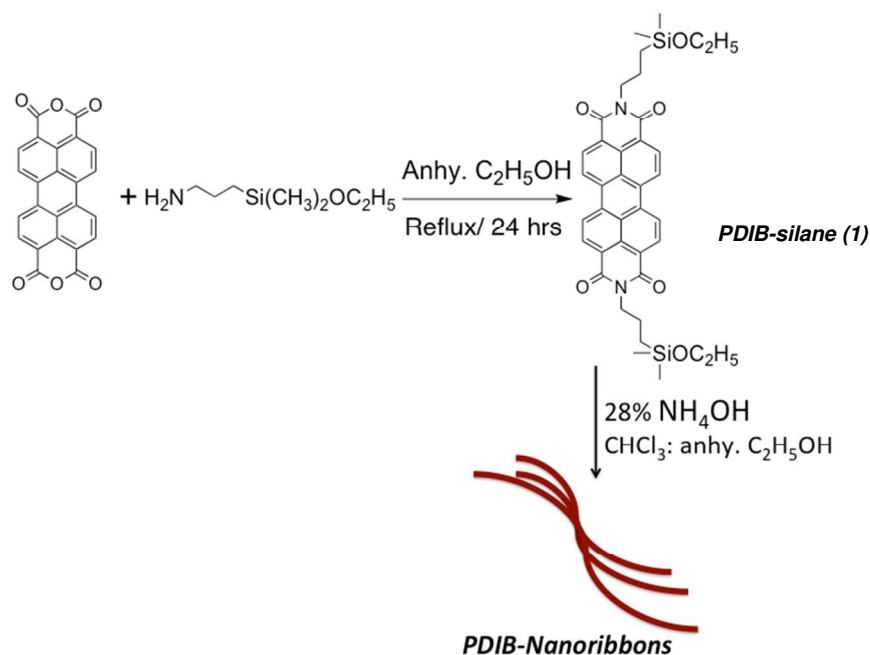
where P_s is intensity of light, J_m is maximum current density and V_m is maximum voltage at maximum power point.

Results and Discussion

PDIB-Nanostructures synthesis: Preparation of perylenediimide-functionalized nanostructures was performed by adapting a modified Stöber method from our previously published work.^{36,37} As depicted in Scheme 1, PDIB-dimethylethoxysilane was synthesized from 3,4,9,10-

tetracarboxyanhydrideperylene and 3-aminopropyl-dimethylethoxysilane. The silane precursor was purified by solvent precipitation to yield pure product of perylenediimidesilane (1). A control experiment was performed and confirmed that insoluble solid removed by precipitation contains hydrolyzed perylenediimide siloxanes.

In a typical procedure, the nanoribbons were prepared by hydrolysis and condensation of PDIB-silane (1) in the presence of NH_4OH in anhydrous ethanol: chloroform 10:1 solvent mixture. The nanoribbons formation was examined under transmission electron microscopy (TEM) as a function of time. In each case, nanoribbons were separated by centrifugation maintaining the rotation speed at 5000 rpm and repeated washing with ethanol. Figure 2 shows the TEM images of nanoribbons formed at different time intervals. The length of nanoribbons depends on the reaction time. The longest nanoribbons (excluding tangled ribbons), with length up to 15 μm , were obtained after 48 hours of reaction time.



Scheme 1. Preparation of PDIB-Nanoribbons

The effect of base concentration for the formation of nanoribbons was studied at a fixed concentration of silane in 10:1 ratio of anhydrous ethanol to chloroform solvent mixture and summarized in Table 1. The results confirmed that base concentration is directly affecting the formation of nanoribbons. At lower base concentration (1.48 mol/L adjusted by adding 2.5 mL deionized water – reaction 2 in Table 1 and entry VI in Table S1), both PDIB-nanorods and spherical nanoparticles were formed. The slight decrease (0.08 mol/L) of base concentration from 1.56 mol/L to 1.48 mol/L resulted in a transition from nanoribbons to nanorods. When the base concentration was lowered to 1.40 mol/L, nanoparticles were abundant and fewer nanorods were present (Table S1 entry IV). On the other hand, the higher base concentration (2.58 mol/L – entry VII in Table S1), gave nanochains, nanorods, or nanoparticles depending on the reaction time. The nanoparticles were more abundant after 48 hrs of reaction time (Figure S2).

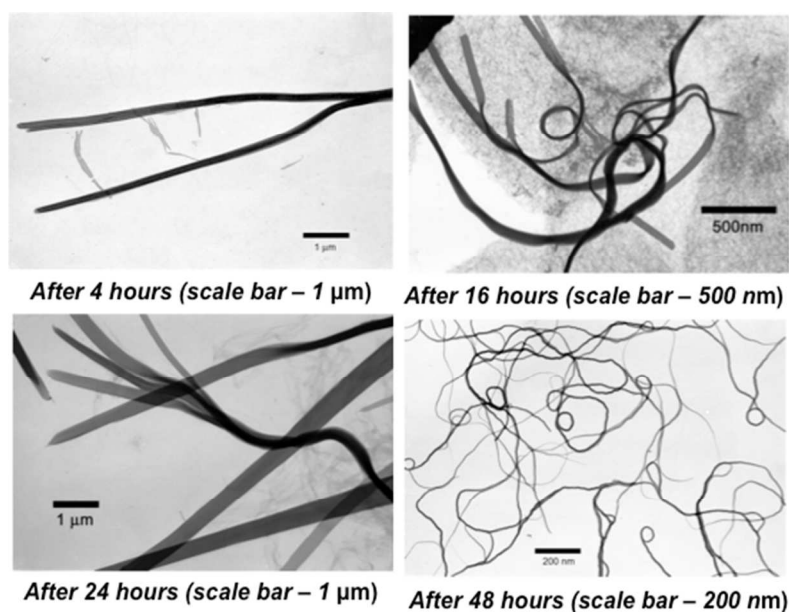


Figure 2. Transmission electron microscopy images of PDIB-nanoribbons at different times

The TEM images reveal that PDIB-nanorods formed at lower base concentration have very smooth surfaces with no spherical nanoparticles present on the nanorod surface. However, nanorods formed at higher base concentration after 16 hrs of reaction time have considerably rougher surfaces with many spherical nanoparticles sticking onto the surface (Figure 3). As shown in Table S1, after running series of reactions under different base concentrations ranging from 1.40 mol/L to 2.58 mol/L, we were able to confirm the optimum base concentrations for the formation of nanoribbons, nanorods and nanochains.

Table 1. The effect of base concentration on the formation of PDIB-nanostructures and their morphologies

Reaction #	Concentration of NH ₄ OH (mol/L)	Dimensions of nanostructures
1	1.56	Nanoribbons - width up to 150 nm and length up to 5µm Nanoparticles – Average size up to 30 nm
2	1.48	Nanorods - width 80-100 nm and length up to 5µm Nanoparticles – Average size range 10-100 nm
3	2.58	Nanochains with length up to 2 µm after 3hs. Nanorods with spherical nanoparticles on nanorod's surface. Width- 100 -200 nm and length up to 9 µm after 4hrs Nanoparticles with the average size range of 20-50 nm after 48 hrs

The amount of PDIB silane (1) used for each reaction is 7×10^{-2} mmol

After running the multiple reactions using these three base concentrations, the TEM results confirmed that the best-suited base concentration for the formation of nanoribbons is 1.56 mol/L per 7×10^{-2} mmol of PDIB-silane (1) in an ethanol to chloroform solvent ratio of 10:1. We performed a series of multiple trial reactions to reproduce the formation of nanoribbons and nanorods using the similar reaction conditions as for reaction 1 and 2 in Table 1 (see supporting

information Table S1). The nanostructures prepared in this manner were isolated after 48 hours and stored as a dry solid and can be redispersed with little sonication in most organic solvents. TEM analysis confirmed that drying did not affect morphology or particle dispersion in organic solvents.

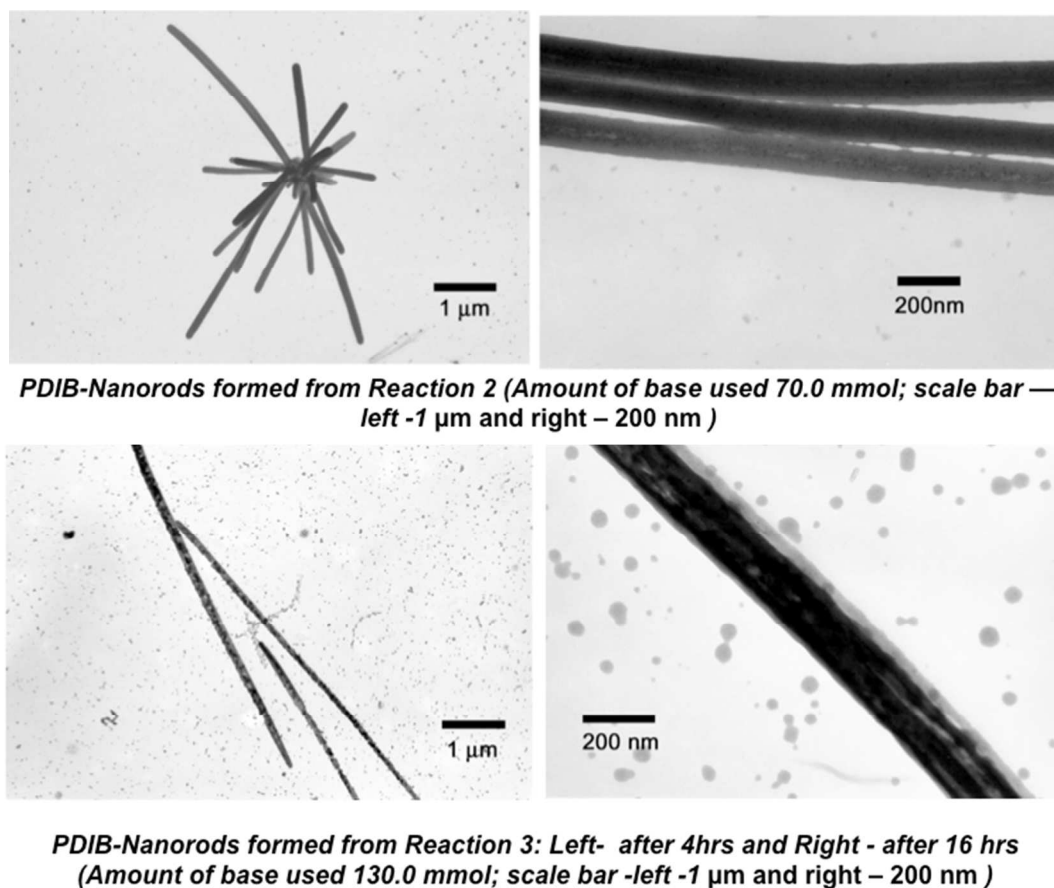


Figure 3: Transmission electron microscopy images of reaction 2 and 3 from the Table 1

The FT-IR spectrum (Figure S3) of PDIB-nanostructures confirmed the presence of characteristic bands for the formation of Si-O-Si bonds and the retention of Si-C linkages during the base-catalyzed hydrolysis and condensation reaction. The alkyl chains -CH and diimide carbonyl stretching vibrations were observed at 2993-2885 and 1692 cm^{-1} , respectively. The presence of aromatic C-C stretching (1593-1553 cm^{-1}) and N-C vibrations (1440 cm^{-1}) further

supports the successful incorporation of perylene-3,4,9,10-tetracarboxylic diimide units to the silsesquioxane core. The well-defined absorption at 1343-1253 cm^{-1} confirms the presence of Si-C bonds in Si-PDI units. The absorption of Si-O-Si was observed at 1098-1016 cm^{-1} , suggesting the formation of a silsesquioxane network.

Photophysical properties of PDIB-nanostructures: The UV-visible absorption and photoluminescence (PL) studies of PDIB-nanoribbons (from Reaction 1 in Table 1) were performed and compared with the spectra of Reaction 2. The photophysical properties of PDIB-nanostructures were studied in chloroform solution. As depicted in Figure 4, the solution phase absorption spectra of PDIB-nanostructures obtained from reactions 1-2 exhibit typical spectral features similar to PDIB-silane monomer **1** with three pronounced peaks with a shoulder around 425 nm, which corresponds to the 0-0, 0-1, 0-2, 0-3 electronic transitions respectively.^{38,39} The transition from ground state to the higher levels of electronic states (0-1, 0-2, and 0-3) are enhanced compared to the 0-0 transition. These spectral changes confirm the strong molecular stacking between PDI moieties similar to the reports previously published for aggregated PDI systems.^{29,39} However, there is no evidence of pronounced absorption band emerging at longer wavelength that indicates no sign of the effective π - π interaction in co-facial configuration of molecular stacking.^{30,40} The fluorescence spectra depict the same peak structures in mirror images of the absorptions with the expected λ_{max} at 532 nm and two vibronic bands at 574 nm and 625 nm (Figure 4). There is some overlapping of the longer wavelength absorption band in the UV absorption spectra and the shorter wavelength emission band in the PL emission spectra. This spectral behavior is typical for aggregated PDI systems as observed previously.^{14,41-43} However, there is no evidence of significant fluorescence quenching that further confirms the lack of π - π electronic coupling.

Thin film fluorescence emission spectra of PDIB-nanoribbons in bulk and as single particles were obtained using the 457 nm and 514 nm output from an Ar⁺ laser and fluorescence was detected using an EMCCD camera. As shown in Figure 5, the fluorescence emission of bulk PDIB nanoribbons in the solid state is red shifted with a broader spectrum compare to its solution phase emissions. However, the emission spectra of single emissive sites in the nanoribbons show well-resolved vibronic bands at 545 nm and 590 nm with a shoulder peak at 640 nm.

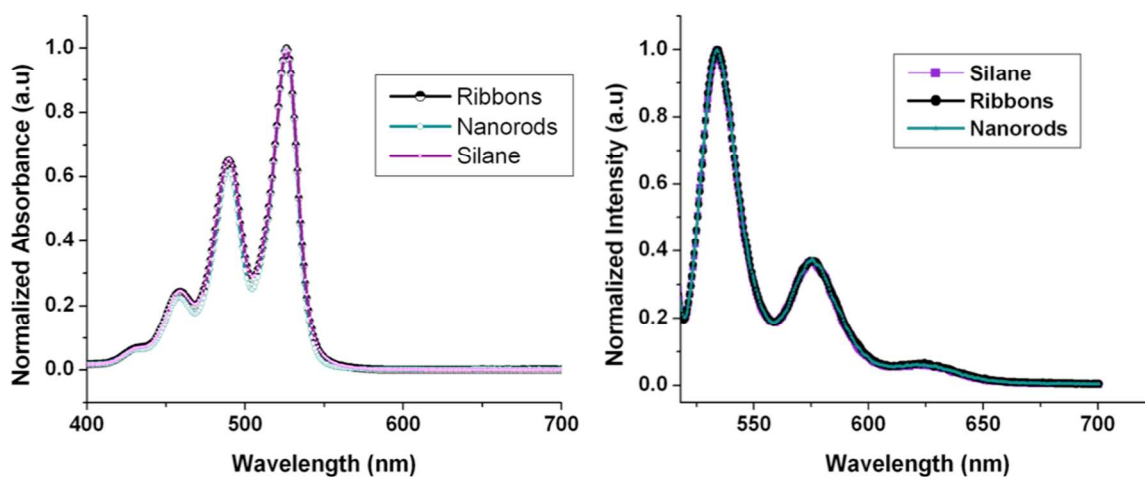


Figure 4. Left - Normalized UV-visible spectra; Right -Normalized PL emission spectra of PDIB-nanostructures (excitation wavelength – 514 nm).

The excited state lifetimes of the nanostructures in ethanol and also in thin films were measured using a ps-pulsed diode laser as the excitation source. The lifetimes of the nanostructures in solution were 3.2 ns and in the thin films 2.7 ns. These values are very close to the excited state lifetimes of other PDI-based molecules. The shorter lifetime in the films suggests some degree of interaction between nanostructures and the thin film.

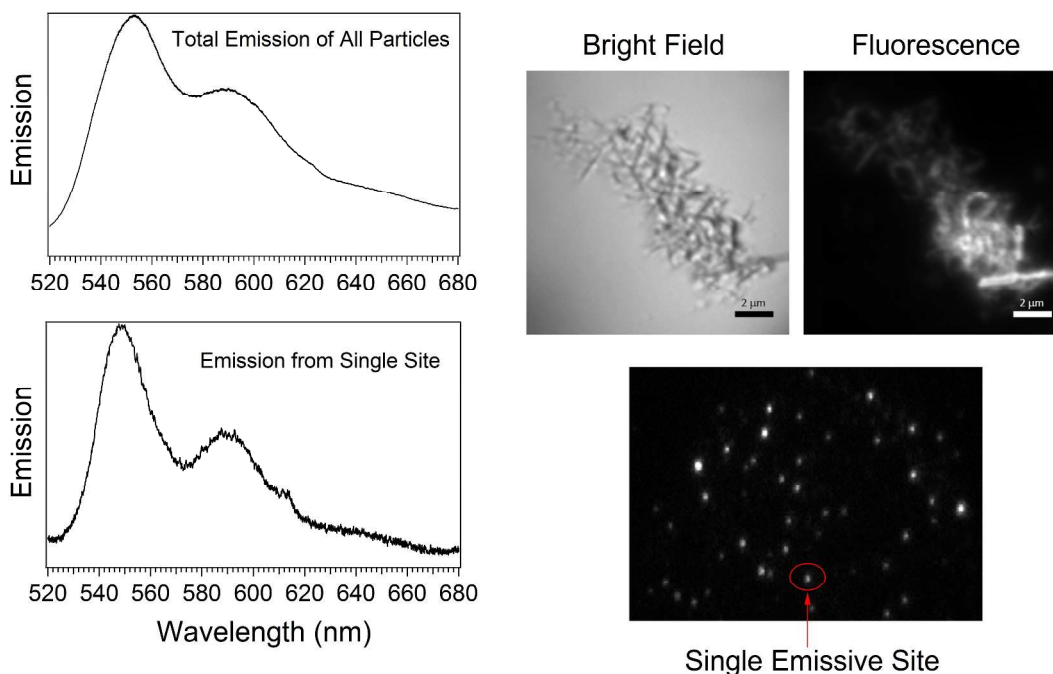


Figure 5. Left: Thin-film fluorescence spectra of bulk and single particle PDIB-nanoribbons. Right-Top: Bright field and fluorescence emission from the same nanoribbons, and Right-Bottom: Emission from single emissive sites in nanoribbons after dilution.

Thin-film morphology of PDIB-nanostructures using Atomic Force Microscopy:

The morphology of the PDIB-nanorods from Reaction 2 was analyzed using the contact-imaging mode of atomic force microscopy (AFM) by means of a silicon nitride tip. Figure 6 shows the 2D and 3D images of the morphology of the thin film containing PDIB nanorods on an area of $40\ \mu\text{m} \times 40\ \mu\text{m}$. It can be seen from the images that the PDIB nanorods are arranged uniformly over the thin film without significant visible agglomeration. However, the nanorods are found to touch each other at one or more points, with very few nanorods staying independent. The 3D image in Figure 6(b) reveals that most of the nanorods are lying flat onto the thin film/substrate due to the influence of gravity. Few nanorods were found at an inclined or near-vertical position, as can be seen from the 3D image of the thin film. The height scale bar of the

scanned images ranges from 0.55 μm to 0.96 μm . The difference in the height bar of the scanned image indicates that the average thickness of the nanorods ranges from 200 – 300 nm. In addition, the lengths of the nanorods have been measured randomly from the scanned images with an average size of 5-6 μm and a range of 3 – 9 μm . More images with different scan sizes and from different areas of thin film were captured and similar results confirmed our findings.

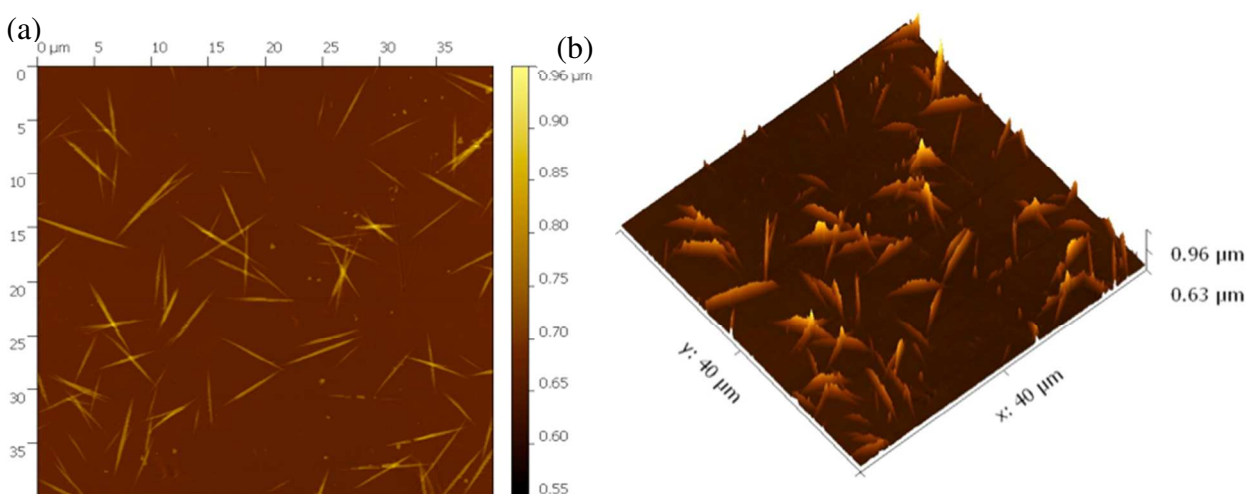


Figure 6. AFM images showing the morphology of the thin film containing PDIB-nanostructures over a scan area of 40 μm x 40 μm : (a) 2D image and (b) 3D image.

Photovoltaic characterization of PDIB-nanostructures: Power conversion efficiencies reported for P3HT/PDI bulk materials are poor due to the formation of macro-crystalline domains and phase segregation.⁴⁴ Previous studies in our group have shown that incorporating PDI units into silsesquioxane network is an effective way to make nano-sized crystalline PDI hybrids with improved PV performance of P3HT/PDI system.³⁶ However, the effect of controlled geometries of PDI-silsesquioxane nanostructures on device performance had not been evaluated in our previous work. Therefore, electrical characterization studies described here may allow us to comprehensively establish how different morphologies with distinct dimensions of PDIB-

silsesquioxane nanostructures affect the photovoltaic performance. Here, we evaluated the photovoltaic performances of two different shapes of PDIB-nanostructures using bulk heterojunction device architecture with P3HT as a donor component. The photovoltaic performance of PDIB nanoribbons and nanorods were characterized using the test devices with the device configuration of ITO/PEDOT.PSS/Blend/Ca-Al. The blends were prepared from the solution of 1:1 mixture of P3HT polymer ($M_w = 30,000-60,000$) and PDIB nanostructures in chlorobenzene. Table 2 summarizes and compares the photovoltaic parameters of the test devices before and after annealing at 100 °C for 5 min.

Table 2. The photovoltaic parameters of PDIB-nanoribbons and PDIB-nanorods

PDIB	PV Parameters at RT			PV Parameters at 100 °C		
	J_{SC} (mA/cm ²)	$V_{OC}(V)$	%PCE	J_{SC} (mA/cm ²)	$V_{OC}(V)$	%PCE
Ribbons	2.01	0.9	0.94	1.80	1.02	0.96
Rods	0.95	0.30	0.16	1.11	0.40	0.26

The current density - voltage curves for devices made from PDIB-nanostructures are shown in Figure 7. The test devices made from PDIB-nanoribbons show higher open circuit voltage (V_{OC}) with fill factor (FF) of 0.42 and short circuit current density (J_{SC}) of 1.80 mA/cm², which did not improve upon annealing the devices to 100 °C. Although blends of nanoribbons gave higher V_{OC} , the power conversion efficiency was 0.96%, which is 0.60% lower than that of for PDIB-nanoparticles reported in our previous work.³⁶ One main reason for the poor performance of the nanoribbons may be the twisted and tangled nature of the ribbons, which led to an unorganized active layer morphology and showed no improvement of film morphology upon annealing. Also, the thickness of the nanoribbons may lower the current density, as the donor-acceptor

interface thickness is critical for charge separation. To confirm the twisted chiral structure of ribbons has impacted on electrical parameters, the electrical conductivity of nanoribbons were measured and compared with the conductivity of the silane precursor. As shown in Figure S9, nanoribbons show low conductivity of 7.3×10^{-3} S/cm, where as the silane precursor shows higher conductivity of 2.11×10^{-2} S/cm. The poor conductivity of nanoribbons compared to its monomer further evidenced that twisted structure has direct impact on electrical properties.

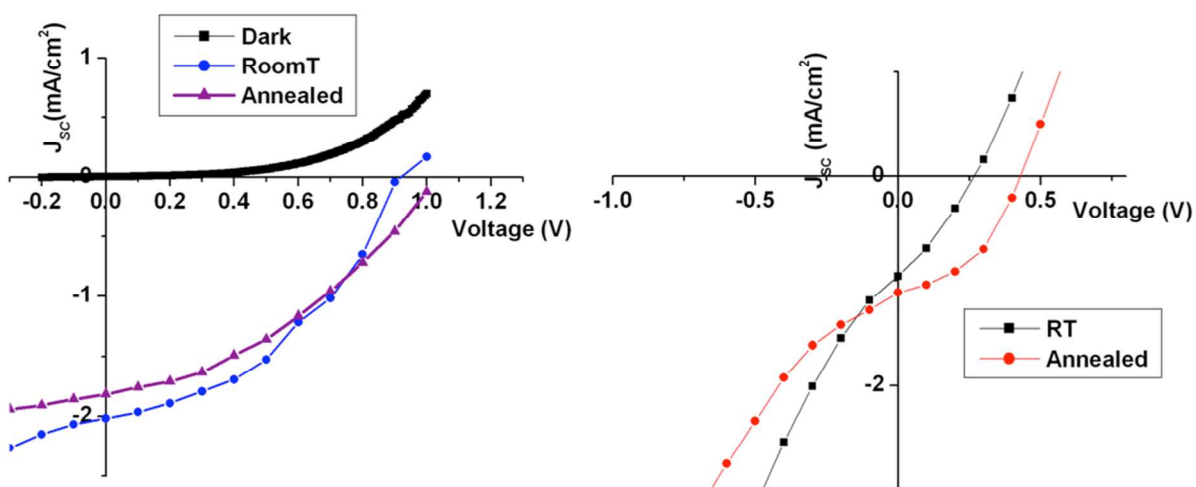


Figure 7. Current density vs voltage curves (J-V) for PDIB-nanoribbons (left) and nanorods (right) at room temperature and after annealed to 100 °C under solar simulator.

The photovoltaic parameters of the devices made from nanorods also resulted in poor performance. The devices composed of nanorods show power conversion efficiency of 0.26% with J_{sc} of 1.11 mA/cm², V_{oc} of 0.40 V, and FF of 0.47 after annealing at 100 °C for 5 min. In contrast to nanoribbons, which show no change in PCE upon annealing, nanorods show improved device performance by ~62% after annealed at 100 °C. The main reason for this increase may be the better ordering of rods within the active layer compare to twisted structure of nanoribbons. However, comparative studies on thin films morphologies at different annealing temperature are necessary to explain this behavior. In order to confirm the test devices are

rectifying and having a diode behavior, the dark current I-V curve along with shunt resistance (R_{sh}) were measured for the test devices made from nanoribbons. The shunt resistance was calculated for multiple test devices using the previously published procedure.⁴⁵ The average shunt resistance ranges from 0.9 - 2.60 $k\Omega/cm^2$ which is in similar magnitude as for typical P3HT/PCBM photovoltaic devices.⁴⁵

These electrical characterizations data suggest that the morphology of PDIB-nanostructures plays an important role on photovoltaic performance. Both nanoribbons and nanorods performed poorly as acceptors for bulkheterojunction solar cells compare to spherical PDIB-silsesquioxane nanoparticles.³⁶ Although power conversion efficiencies of ribbons and rods are very low, the current work has direct implication in evaluating the effect of structural morphology on PV performance and in developing better PDI-silsesquioxane nanomaterials, which can enhance the device performance of P3HT/PDI donor-acceptor system in the future.

Conclusion

We demonstrated a convenient method to prepare organic semiconductors-functionalized nanostructures through the covalent synthesis of perylenediimide-functionalized silsesquioxane nanoribbons (PDIB-nanoribbons) and nanorods (PDIB-nanorods). The formation of nanoribbons and nanorods was controlled by varying the base concentration. The slight decrease in the base concentration (0.08 mol/L) resulted the morphology change from nanoribbons to nanorods. Although both nanostructures showed poor performance as acceptors in bulk heterojunction solar cells, we believe that the method described here could be useful to make wide variety of ligand-functionalized nanostructures from appropriately functionalized monoalkoxysilane precursors. Because this is a unique example for making nanostructures having controlled morphologies using covalent synthesis, we believe these findings will contribute to the development of novel functional nanomaterials for organic electronics.

Acknowledgements

The authors gratefully acknowledge the financial support from Office of Research Foundation at WKU (RCAP- 13-8042), Kentucky Science & Engineering Foundation (KCF-KSTC-144-401-13-062) and from the National Science Foundation (CHE-0955550 and EPS-0903787). We are also pleased to acknowledge Dr. John Andersland for SEM and TEM support and Pauline Norris at Advanced Materials Institute for elemental analysis.

Notes and references

^aDepartment of Chemistry, Western Kentucky University, Bowling Green, KY 42101;

^bDepartment of Chemistry & Biochemistry, University of Mississippi, MS 38677;

^cDepartment of Architectural & Manufacturing Sciences, Western Kentucky University, Bowling Green, KY 42101.

*Corresponding Authors: Hemali Rathnayake –Department of Chemistry, Western Kentucky University, Bowling Green, KY 42101, Hemali.rathnayale@wku.edu; Tel. Phone – 270-745-6238.

Nathan I Hammer –Department of Chemistry & Biochemistry, University of Mississippi, MS 38677, nhammer@olemiss.edu; Tel. Phone - 662-915-3989.

† Electronic Supplementary Information (ESI) available: Experimental procedures are available in supporting information section. See DOI: 10.1039/b000000x/.

1. S. Guo, J. Li, W. Ren, D. Wen, S. Dong, E. Wang, *Chem. Mater.* 2009, **21**, 2247–2257.
2. Q. Ji, R. Iwaura, M. Kogiso, J. H. Jung, K. Yoshida, T. Shimizu, *Chem. Mater.* 2004, **16**, 250–254.
3. B. Q. Wei, R. Vajtai, Y. Jung, J. Ward, R. Zhang, G. Ramanath, P. M. Ajayan, *Chem. Mater.* 2003, **15**, 1598–1606.
4. B. C. Satishkumar, S. K. Doorn, G. A. Baker, A. M. Dattelbaum, *ACS Nano* 2008, **2**, 2283–2290.

5. R. S. Norman, J. W. Stone, A. Gole, C. J. Murphy, T. L. Sabo-Attwood, *Nano Lett.* 2008, **8**, 302–306.
6. S. Kim, S. K. Kim, S. Park, *J. Am. Chem. Soc.* 2009, **131**, 8380–8381.
7. M. S. Fuhrer, B. M. Kim, T. Dürkop, T. Brintlinger, *Nano Lett.* 2002, **2**, 755–759.
8. A. Züttel, P. Sudan, P. Mauron, T. Kiyobayashi, C. Emmenegger, L. Schlapbach, *Int. J. Hydrogen Energy* 2002, **27**, 203–212.
9. P. X. Huang, F. Wu, B. L. Zhu, X. P. Gao, H. Y. Zhu, T. Y. Yan, W. P. Huang, S. H. Wu, D. Y. Song, *J. Phys. Chem. B* 2005, **109**, 19169–19174.
10. X. Duan, C. M. Lieber, *Adv. Mater.* 2000, **12**, 298–302.
11. J. W. Grebinski, K. L. Richter, J. Zhang, T. H. Kosel, M. Kuno, *J. Phys. Chem. B* 2004, **108**, 9745–9751.
12. R. Adelung, O. C. Aktas, J. Franc, A. Biswas, R. Kunz, M. Elbahri, J. Kanzow, U. Schürmann, F. Faupel, *Nat Mater* 2004, **3**, 375–379.
13. S. Milenkovic, A. W. Hassel, A. Schneider, *Nano Lett.* 2006, **6**, 794–799.
14. Z. Zhou, J. L. Brusso, S. Holdcroft, *Chem. Mater.* 2010, **22**, 2287–2296.
15. E. W. Meijer, A. P. H. J. Schenning, *Nature* 2002, **419**, 353–354.
16. F. J. M. Hoeben, P. Jonkheijm, E. W. Meijer, A. P. H. Schenning, *J. Chem. Rev.* 2005, **105**, 1491–1546.
17. G. B. W. L. Ligthart, H. Ohkawa, R. P. Sijbesma, E. W. Meijer, *J. Am. Chem. Soc.* 2005, **127**, 810–811.
18. V. Berl, M. Schmutz, M. J. Krische, R. G. Khoury, J.-M. Lehn, *Chem. Eur. J.* 2002, **8**, 1227–1244.
19. C. F. J. Faul, M. Antonietti, *Adv. Mater.* 2003, **15**, 673–683.

20. G. C. L. Wong, J. X. Tang, A. Lin, Y. Li, P. A. Janmey, C. R. Safinya, *Science* 2000, **288**, 2035–2039.
21. J. M. Lehn, *Science* 2002, **295**, 2400–2403.
22. J. H. Ryu, D. J. Hong, M. Lee, *Chem. Commun.* 2008, 1043–1054.
23. H. J. Kim, Y. B. Lim, M. Lee, *J. Polym. Sci., Part A: Polym. Chem.* 2008, **46**, 1925–1935.
24. J. H. Fuhrhop, T. Wang, *Chem. Rev.* 2004, **104**, 2901–2938.
25. T. Shimizu, M. Masuda, H. Minamikawa, *Chem. Rev.* 2005, **105**, 1401–1444.
26. L. C. Palmer, S. I. Stupp, *Acc. Chem. Res.* 2008, **41**, 1674–1684.
27. M. Antonietti, S. Förster, *Adv. Mater.* 2003, **15**, 1323–1333.
28. M. Lazzari, M. A. López-Quintela, *Adv. Mater.* 2003, **15**, 1583–1594.
29. F. Würthner, *Chem. Commun.* 2004, 1564–1579.
30. K. Balakrishnan, A. Datar, R. Oitker, H. Chen, J. Zuo, L. Zang, *J. Am. Chem. Soc.* 2005, **127**, 10496–10497.
31. A. Datar, K. Balakrishnan, X. Yang, X. Zuo, J. Huang, R. Oitker, M. Yen, J. Zhao, D. M. Tiede, L. Zang, *J. Phys. Chem. B* 2006, **110**, 12327–12332.
32. Y. Che, A. Datar, K. Balakrishnan, L. Zang, *J. Am. Chem. Soc.* 2007, **129**, 7234–7235.
33. A. L. Briseno, S. C. B. Mannsfeld, C. Reese, J. M. Hancock, Y. Xiong, S. A. Jenekhe, Z. Bao, Y. Xia, *Nano Lett.* 2007, **7**, 2847–2853.
34. L. Zang, Y. Che, J. S. Moore, *Acc. Chem. Res.* 2008, **41**, 1596–1608.
35. G. De Luca, A. Liscio, P. Maccagnani, F. Nolde, V. Palermo, K. Müllen, P. Samorì, *Adv. Funct. Mater.* 2007, **17**, 3791–3798.

36. H. Rathnayake, J. Binion, A. McKee, D. J. Scardino, N. I. Hammer, *Nanoscale* 2012, **4**, 4631–4640.
37. H. Rathnayake, N. Wright, A. Patel, J. Binion, L. E. McNamara, D. J. Scardino, N. I. Hammer, *Nanoscale* 2013, **5**, 3212–3215.
38. S. M. Lindner, M. Thelakkat, *Macromolecules* 2004, **37**, 8832–8835.
39. K. Balakrishnan, A. Datar, T. Naddo, J. Huang, R. Oitker, M. Yen, J. Zhao, L. Zang, *J. Am. Chem. Soc.* 2006, **128**, 7390–7398.
40. P. M. Kazmaier, R. Hoffmann, *J. Am. Chem. Soc.* 1994, **116**, 9684–9691.
41. M. J. Ahrens, L. E. Sinks, B. Rybtchinski, W. Liu, B. A. Jones, J. M. Giaimo, A. V. Gusev, A. J. Goshe, D. M. Tiede, M. R. Wasielewski, *J. Am. Chem. Soc.* 2004, **126**, 8284–8294.
42. E. Hädicke, F. Graser, *Acta Crystallogr., Sect. C: Cryst. Struct. Commun.* 1986, **42**, 189–195.
43. J. Feng, B. Liang, D. Wang, H. Wu, L. Xue, X. Li, *Langmuir* 2008, **24**, 11209–11215.
44. S. Rajaram, P. B. Armstrong, B. J. Kim, J. M. J. Fréchet, *Chem. Mater.* 2009, **21**, 1775–1777.
45. J. H. Lee, S. Cho, A. Roy, H. T. Jung, A. J. Heeger, *Appl. Phys. Lett.* 2010, **96**, 163303–163303–3.